Rangelow, Ivo W.; Ivanov, Tzvetan; Ahmad, Ahmad; Kästner, Marcus; Lenk, Claudia; Bozchalooi, Iman S.; Xia, Fangzhou; Youcef-Toumi, Kamal; Holz, Mathias; Reum, Alexander:

Review Article: Active scanning probes: a versatile toolkit for fast imaging and emerging nanofabrication

Original published in:	Journal of vacuum science & technology / B. - New York, NY : Inst. - 35 (2017), 6, art. 06G101, 14 pp.
Original published:	2017-11-03
ISSN:	2166-2754
DOI:	10.1116/1.4992073
[*Visited:*	2019-04-01]

REVIEW ARTICLE

Review Article: Active scanning probes: A versatile toolkit for fast imaging and emerging nanofabrication

Ivo W. Rangelow,[a] Tzvetan Ivanov, Ahmad Ahmad, Marcus Kaestner, and Claudia Lenk
Department of Micro- and Nanoelectronic Systems (MNES), Ilmenau University of Technology, Gustav-Kirchhoff-Str. 1, 98693 Ilmenau, Germany

Iman S. Bozchalooi, Fangzhou Xia, and Kamal Youcef-Toumi
Department of Mechanical Engineering, Massachusetts Institute of Technology, 77 Massachusetts Avenue, Cambridge, Massachusetts 02139

Mathias Holz and Alexander Reum
Nano Analytik GmbH, Ehrenbergstraße 1, 98693 Ilmenau, Germany

(Received 26 June 2017; accepted 18 August 2017; published 3 November 2017)

With the recent advances in the field of nanotechnology, measurement and manipulation requirements at the nanoscale have become more stringent than ever before. In atomic force microscopy, high-speed performance alone is not sufficient without considerations of other aspects of the measurement task, such as the feature aspect ratio, required range, or acceptable probe-sample interaction forces. In this paper, the authors discuss these requirements and the research directions that provide the highest potential in meeting them. The authors elaborate on the efforts toward the downsizing of self-sensed and self-actuated probes as well as on upscaling by active cantilever arrays. The authors present the fabrication process of active probes along with the tip customizations carried out targeting specific application fields. As promising application in scope of nanofabrication, field emission scanning probe lithography is introduced. The authors further discuss their control and design approach. Here, microactuators, e.g., multilayer microcantilevers, and macroactuators, e.g., flexure scanners, are combined in order to simultaneously meet both the range and speed requirements of a new generation of scanning probe microscopes. https://doi.org/10.1116/1.4992073

I. INTRODUCTION

In order to unlock some of the important potentials of nanotechnology, next generation scanning probe technologies are focusing on a throughput compliance for emerging nanoscale analysis and nanofabrication. Furthermore, the functionality of scanning probe technologies is steadily increasing, which leads to novel application areas. This trend is driving new paradigms of processes based on scanning probes, enabled by innovative new probes and imaging methods. The upcoming applications are demanding for high-speed imaging and nanofabrication solutions. As such, the scanning probe technology has to follow up.

For the first time, Butt *et al.*[1] described the scan speed limits of atomic force microscopy (AFM). On the basis of his considerations, which described the role of the cantilever and scanner for high speed imaging, many researchers focused on optimization of the control electronics bandwidth (BW) in order to track surface topography changes as fast as possible. This helped mainly in case of flat surfaces, e.g., imaging of DNA on Mica substrate.[2] Furthermore, optimization of scanner properties by using stiffer and compressed Z-piezo-stacks have contributed to bandwidth improvements of actuation in the vertical direction, which has resulted in significantly improved imaging speeds.[3–6]

Another approach to establish high-speed AFM is based on reducing the size of the AFM cantilevers, a development that started in 1993.[7,8] As a result, short cantilevers (23 × 12 μm) have been developed. By using optical deflection detection, a single topographic AFM image of DNA was obtained within 1.7 s.[9] Ando *et al.*[3] achieved an image rate of 12.5 frames/s by a novel high-speed AFM system. In particular, Myosin V molecules were scanned in water using a novel high-speed scanner (scan range of 240 nm) and fast controlling setup. For this purpose, small cantilevers with resonance frequencies of 600 kHz, measured by optical detection, were employed. Further development and characterization of small cantilevers was continued by Yun-Peng Song *et al.*[10] and Ando *et al.*,[3] which enabled higher resonance frequencies and relaxed the limitations with respect to the response time of the force sensor.

A common approach for probe measurement is based on optical read-out.[11] However, the shortcomings of optical detection, associated with diffraction and reduced sensitivity,

[a]Electronic mail: ivo.rangelow@tu-ilmenau.de

necessitate the development of novel measurement methods to quantify probe–sample interactions. Due to the optical read-out, the dimensional downscaling of conventional scanning probes reaches its limits. In particular, a minimum reflective area is required on the cantilever beam backside, in the range of $3 \times 9\,\mu$m in high-end AFM systems facilitating a small laser spot.[12] Hence, the direct integration of read-out and actuation onto the cantilever is essential for further miniaturization.

In this context, self-sensing probes have the potential to overcome the optical read-out limitations. Typically, a piezo-resistivity based deflection sensor is integrated into the cantilever beam itself.[13] Actuation can be obtained, for example, thermomechanically.[13] The so called active scanning probe technology integrates both bending read-out as well as actuation capability. In terms of the technological development of AFM systems, the cantilever evolved from a simple passive deflection element to a complex microelectromechanical system through integration of functional groups, such as piezoresistive detection sensors and thermomechanical actuators. Thereby, the deflection sensor is carefully thermally isolated from the actuator and designed for minimum electronic crosstalk. Active cantilevers allow the measurement of surface topology and related surface characteristics, whereby the integrated actuation enables the control of the tip position. Here, the system is even capable to measure the thermo-mechanical noise of the cantilever.[14] The progress of active cantilever development has resulted in a significant downscaling of the cantilever system, which is linked to a reduction in cantilever mass and increase of resonance frequency (f_c) to spring constant (k_c) ratio, summarized in Fig. 1.

Recent trends, associated developments, and miniaturization efforts of the active cantilever technology are reviewed in more detail in Refs. 12 and 15. One of our main research targets has been to further extend self-sensing and self-actuating probe capabilities to achieve the requirements of high speed imaging. The general development history of our active cantilever was presented already in 2014.[15] For high-speed AFM imaging, we follow the two approaches

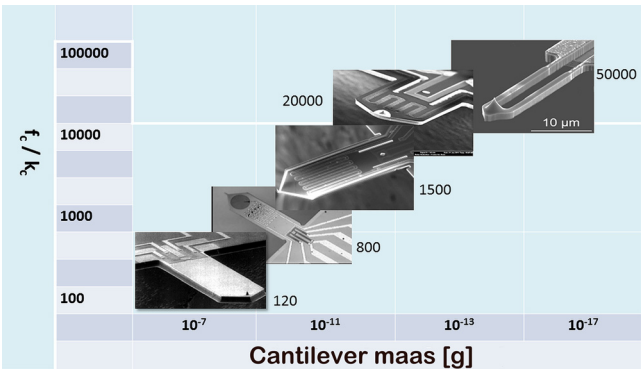

FIG. 1. (Color online) Development of active cantilever technology toward high speed imaging applications. The different active cantilever systems, which are developed at nanoanalytik GmbH and TU-Ilmenau, are plotted as function of cantilever mass vs ratio of resonance frequency (f_c) to spring constant (k_c). The numbers besides the cantilever indicate the f_c to k_c ratio.

described earlier, i.e., optimizing the active cantilevers and the development of high-speed, large range nanopositioning stages with appropriate control. In this context, active cantilever with higher resonance frequency, higher bandwidth, and low spring constant will be presented. To improve the force sensitivity and measurement throughput (speed), we increased the ratio of the resonance frequency to spring constant. In other words, we aimed to fabricate softer and smaller probes, which feature faster imaging dynamics and reduced probe–sample interaction forces while maintaining a high sensitivity. Furthermore, it has been shown that, even with static thermal time constant of $30\,\mu$s, high resonance frequencies of up to 4 MHz can be addressed through thermomechanical actuation.[15] Thermal actuation, due to simple implementation and extraordinary dynamic behavior, is an excellent candidate for self-actuated high frequency cantilever sensors. Herein, the authors describe in this paper in more detail our efforts in the development of miniaturized active cantilevers.

Large range and high-speed scan performance is furthermore required by the application of active cantilevers for controlled nanomanufacturing, fast imaging, metrology, and characterization. These features are combined in a scanning probe based tool developed by our team during the last two decades. Due to the versatile maskless patterning possibilities for sub-10 nm resolution, at relatively low cost, numerous tip-based nanofabrication methods have been developed in the last 30 years.[16] For instance, field emission scanning probe lithography (FE-SPL), emerged from our group, is a very promising candidate offering routinely a resolution below 10 nm,[17,18] an overlay accuracy below 1 nm,[19] and relatively low equipment costs.[17,18] Moreover, scanning probes provide a multi-nano-toolbox for closed-loop lithography, which incorporates ultrahigh overlay alignment, *in situ* inspection and analysis capabilities as well as respective feature functionalization. In this term, FE-SPL is suited for rapid nanoscale prototyping, fabrication of 1:1 masks for nanoimprint lithography (NIL), or creation of property-defining nanodevice features at the single digit level. To overcome the throughput limitations of a single probe, already developed scale-up strategies of parallel probes based on the self-actuation and self-sensing concepts.

The applications mentioned earlier further necessitate achievement of large-range in addition to high speed scan performance. In particular, a large scan range in lateral direction is needed in order to cover at least the spacing between the individual probes of a self-sensed probe array. In this form, a complete overlap of neighboring scan fields can be achieved. Similarly, in the vertical direction, the speed and range specification should fulfill the requirements of recent high-aspect ratio features. Unlike applications in biology and medicine, in which high-speed performance of AFM is needed only in a small scan range (e.g., typical feature sizes in range of a few nanometers in the vertical and hundreds of nanometers in the lateral directions[3]), in the field of micro/nanoelectronics, nanomanufacturing, and quality control, the range requirements are more stringent. Here, one essential part of our developments has been focused on the

design and control of high-speed, large range nanopositioning stages. These scanner types merge the high-speed performance of shorter-range actuators with the large-range performance of their slower counter parts. By properly designing the associated control, one can benefit from both types of actuators in simultaneously achieving large range and high-speed performance.[4,5,20] Due to the complications associated with dynamic coupling of such multicomponent scanners, the control design is often too complex for daily applications in microscopy technologies where users are often unaware of the control design intricacies. Proportional–integral–derivative (PID) controllers are widely accepted by users due to their simplicity. Several earlier works in the field have attempted to implement multiactuated scanner designs and the associated control strategies such as data-driven PID approach foo multi-actuated scanner[21,22] and induced vibration contact detection jumping mode operation[23] for high-speed and large range performance. However, due to the controller and operation complexity, the previously proposed solutions have not successfully found their way to the microscopy industry and into the hands of scientists using these microscopes. As will be discussed later, in our approach, we followed a parallel approach for scanner design and control, where the scanner is designed for controllability by minimizing the expected dynamic coupling. The designed controller, although potentially very complex in terms of handling dynamics, appears from the user perspective as simple as a PID.[20] With combined high speed and large range scanning capability, a large range overview of the sample can be obtained and moreover, high frame rate imaging of a zoomed-in local area can be achieved. When combined with active probe sensor arrays, the performance of high-speed large-range AFM system can be significantly improved.

In Sec. II, we will present an overview of active cantilever properties, manufacturing, application and optimization for high-speed AFM. In Sec. III, we will focus on scanner optimization for high-speed AFM by first explaining important parameters to describe high-speed performance of SPL tools and, second, addressing scanner design issues and solutions, in particular, for the usage of active probe arrays.

II. SELF-SENSING AND SELF-ACTUATED PROBES AND ARRAYS

A. Piezoresistive read-out

The self-sensing capability, based on the piezoresistive effect, was first introduced in 1991 by Tortonese *et al.*[24] at Stanford University. He demonstrated atomic resolution potential of these sensors. Piezoresistive cantilevers usually use thin *p* doped resistors positioned at high stress locations lengthwise on the bending beam.[25] Due to the piezoresistive effect, mechanical stress, which is induced within the resistors, leads to changes in their specific resistance. By biasing via a fixed current, this change is converted into an electrical voltage signal. The stress sensitivity of the p-doped resistors depends linearly on the operating current. However, such sensors require sophisticated electronics to minimize parasitic effects and temperature drift as well as to increase the signal-to-noise ratio. In this context, polycrystalline silicon as electrical shield could also be used to reduce noise effects and improve temperature sensitivity.[26]

A significant improvement in performance of such cantilevers with respect to piezoresistive deflection sensitivity and temperature stability has been achieved by using an integrated Wheatstone bridge configuration.[25,27] Here, effective crosstalk isolation and temperature drift compensation have been employed. Furthermore, due to the optimized piezoresistor technology, a significantly improved signal to noise ratio was achieved leading to current sensitivities and force gradient resolution, which are equal to the optical read-out techniques.[28,29] By application of these cantilever types, AFM measurements with high scanning speeds of up to 200 lines/s have been shown (Fig. 2). In that case, we used the AFM set-up presented earlier.[30]

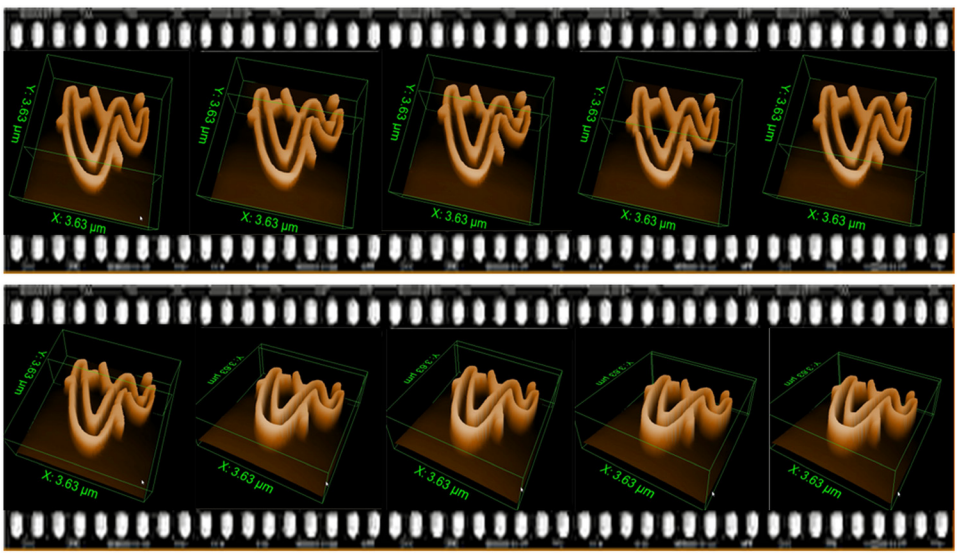

FIG. 2. (Color online) AFM image achieved with high speeds (256 lines/s). The height of the features was 220 nm. The AFM measurement set-up was presented in Ref. 30.

1. Determination of piezoresistive read-out noise

We used the following approach in order to determine the piezoresistive read-out system noise: (1) recording of the amplitude-distance curve; (2) performing a virtual scan in air, without tip-sample interactions, and recording of the corresponding amplitude image. The minimum detectable cantilever deflection is derived. As shown in Fig. 3, the calibration factor K of a cantilever oscillation is determined by the amplitude-distance curve

$$K = \frac{\Delta z}{\Delta v} = \frac{10\,\text{nm}}{220\,\text{mV}} = 0.045\,\text{nm/mV}, \tag{1}$$

with Δz is the change of the relative tip-sample distance in nanometer) and v is the associated amplitude change in millivolt.

Based on K [Eq. (1)], the free oscillation amplitude A_f of the cantilever in nanometer (AFM amplitude image is taken in air) could be calculated, by using Eq. (2),

$$\begin{aligned} A_f(\text{nm}) &= A_f(\text{mV}) \cdot K = 900\,\text{mV} \cdot 0.045\,\text{nm/mV} \\ &= 40.5\,\text{nm}. \end{aligned} \tag{2}$$

Afterward, the AFM amplitude image is acquired with a lock-in bandwidth of 1 kHz. Therefrom, the RMS noise in millivolt is determined. In this particular example, an RMS noise of 0.347 mV is measured.

The RMS noise in nanometer is calculated by using the cantilever calibration factor K_f of Eq. (1),

$$\text{Noise} = \text{RMS} \cdot K = 0.347\,\text{mV} \cdot 0.045\text{nm/mV} = 0.15\,\text{Å}. \tag{3}$$

B. Thermomechanical actuation

The method of thermomechanical actuation[31] is based on a multilayer structure, which is exposed to a temperature increase. Thermomechanical actuation, also called bimorph actuation, requires a sandwich structure of at least two materials featuring a mismatch of thermal expansion coefficients. If heat is locally applied, the beam experiences a deflection. The heating can be achieved by a focused laser beam[32] or by Joule heating through an integrated resistor.[28] Due to tailoring of the material properties of the probes, a static displacement in range of 10 μm has been realized.[14] This was achieved by decreasing of the silicon layer thickness, combined with an enhancement of the thermal expansion coefficient of the actuator material (Al + Mg). The boosted thermal expansion mismatch leads to increased actuation efficiencies, but also to amplified cross-sensitivities with respect to environmental temperature fluctuations. This could be a source of low-frequency noise like environmental noise, such as humidity/temperature instabilities and 1/f noise in the signal amplifying electronics. A finite element method model has been used to evaluate the static as well as dynamic behavior of the bimorph structure. It has been shown that even with static thermal time constants of 30 μs, high resonance frequencies of up to 4 MHz can be achieved. Associated simulation results are published in Ref. 33, wherein the maximum temperature response of the cantilever body as a result of a 1 MHz square wave of heat generation power is investigated.

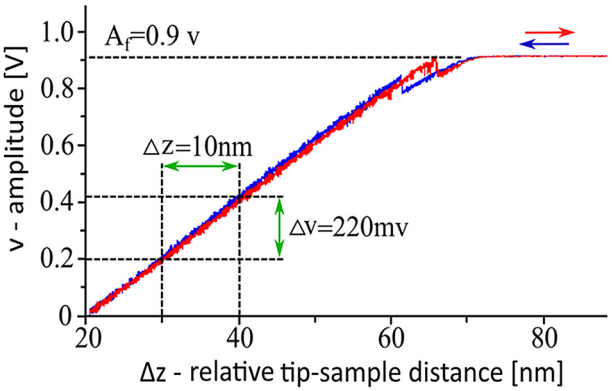

FIG. 3. (Color online) Amplitude distance curve (blue, approach; red, retraction). The experiments are carried out with an AC actuation amplitude of 60 mV, DC actuation of 60 mV, and a drive frequency of 10.164 kHz.

C. Fabrication of active cantilever probes

Thermomechanically actuated piezoresistive AFM probes are fabricated by using (1) a surface micromachining process in order to form sharp tips, (2) standard IC planar processing, (3) silicon on insulator (SOI)–wafers, and (4) bulk micromachining to form the cantilever membrane. AFM tips are defined at the beginning of the fabrication process on top of the SOI layer.[15] First, 4 in. n-Si $\langle 100 \rangle$ wafers are oxidized, and lithography for tip formation is done. Reactive ion etching (RIE) with double resist, a SiO_2 mask, and Ar-SF_6 plasma are used to create mesa islands at places where the free end of the cantilever should be. Next, sharp tips are formed by RIE and/or wet etching based undercuts. Since the tips are fabricated in the beginning, a protective coating is necessary in order to preserve the tips during subsequent processing. Therefore, the tips are covered with a Si_xN_y layer. The nitride film, covered with photoresist, is used subsequently as a mask for boron implantation at 30 keV in order to define the electrical leads to the Wheatstone bridge. Microwave O_2-plasma stripping removes the resist layer, followed by an annealing process at 1050 °C for 30 min. The piezoresistors, arranged in a Wheatstone bridge, are defined by boron implantation at 20 keV with subsequent rapid thermal annealing (RTA) at 1100 °C for 30 s. Herein, resistors created by boron implantation in ultrahigh vacuum, followed by RTA, offer best performance. The deposition of a 150 nm thick zero-stress Si_3N_4 layer by plasma enhanced chemical vapor deposition passivates the front side of the wafer. This layer is removed locally from contact pads, which were previously highly doped, by a plasma etching process. The deposited and subsequently patterned aluminum (Al) thin film forms the leads as well as the microheater of the bimorph actuator. An annealing step in N_2 atmosphere at 410 °C for 50 min is carried out. At the backside of the wafer, the oxide layer is patterned and etched down to the silicon substrate using a gas chopping reactive ion etching

(GChRIE) process.[13] Tetramethylammoniumhydroxide solution is applied for wet anisotropic etching in order to define the cantilever membrane. The cantilever beam is formed from the front side of the wafer (side, at which the tips are initially defined) through GChRIE using a thick resist mask. Finally, a thick layer of Al is deposited at the backside of the wafer for enhanced actuation. Microwave plasma stripping removes the resist. The AFM cantilever or arrays are mechanically separated from the remaining silicon frame.

D. Tailoring toward specific applications: Modification of active probe tips

On the basis of the active cantilever probes, shown as an example in Fig. 4, diverse cantilever modifications have been developed, tailored to specific applications. Scanning probe microscopy (SPM) is beneficial to reproducible fabrication of the cantilever sensors for mechanical, electrical, optical, thermal, and chemical material characterization with highest lateral and/or time resolution. Using combined CMOS and MEMS techniques, several types of active cantilevers and tips have been demonstrated.[12] We introduce in 1994 the Wheatstone bridge configuration[25] for the piezoresistive readout and later on the thermomechanical actuation. All following developments were focused only on tip functionalization as shown in Fig. 7.

Over time these active cantilever types have evolved, as summarized in Figs. 5 and 6. Figure 5 shows ultrasmall, high frequency cantilever types, and Fig. 6 gives an overview on various tip modifications integrated on standard active cantilever for use in different application fields. The following application fields were addressed by active cantilever sensors:

(1) Mass detection [Fig. 6(a)]: The mass sensitivity depends on the effective mass of the sensor, the Young's modulus, as well as the sensor's geometry. The detected amount of mass was only 4.67×10^{-18} kg at room temperature.
(2) Scanning thermal microscopy [SThM, Figs. 6(b), 6(c), and 6(n)]: The SThM is a member of the SPM family, which offers higher sensitivity and more advantages over conventional thermal measurement methods. In comparison to most of SThM probes, we fabricated active sensors with self-actuating and self-sensing capabilities to avoid any optical setup. Employing conventional MEMS fabrication and a focused ion beam milling processing, novel thermal sensitive probes have been fabricated [Fig. 6(b)]. The fabricated thermal

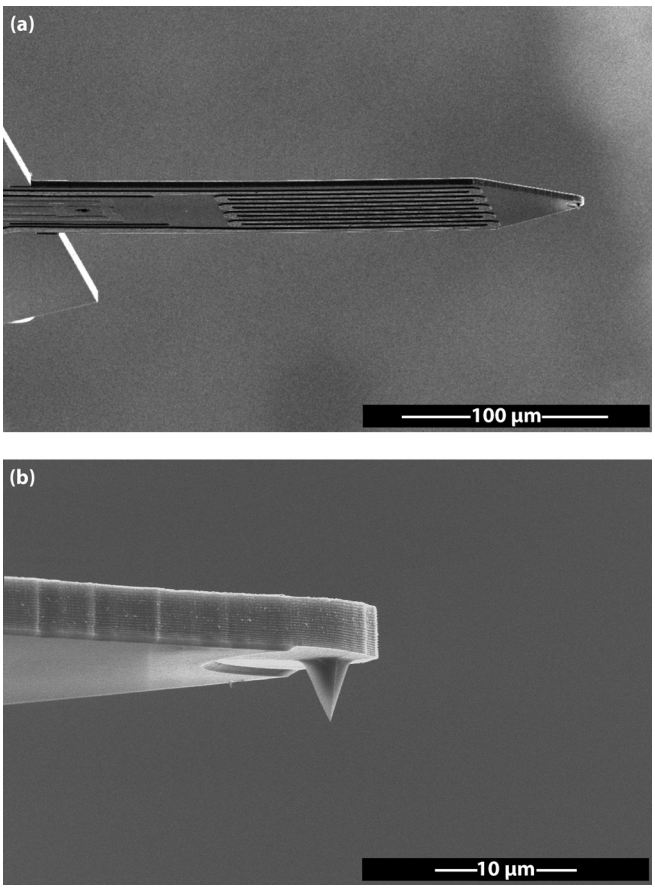

FIG. 4. SEM side view image of the active cantilever probes. Piezoresistive read-out and thermomechanical actuation are integrated. A sharp 5.6 μm high silicon tip (b) at the end of the cantilever (a) ensures advanced AFM imaging capabilities.

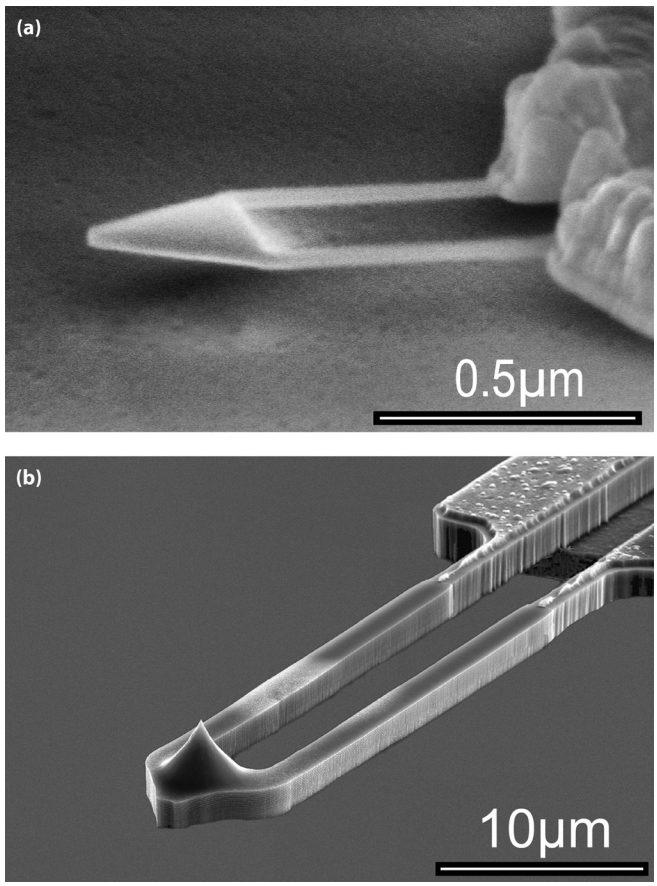

FIG. 5. Ultrasmall, high frequency cantilever fabricated. (a) SEM image of 112 MHz piezoresistive cantilever with 14 nm wide legs, applied for mass detection; (b) SEM image of 2.3 MHz active two-leg cantilever with integrated AFM tip for surface measurements.

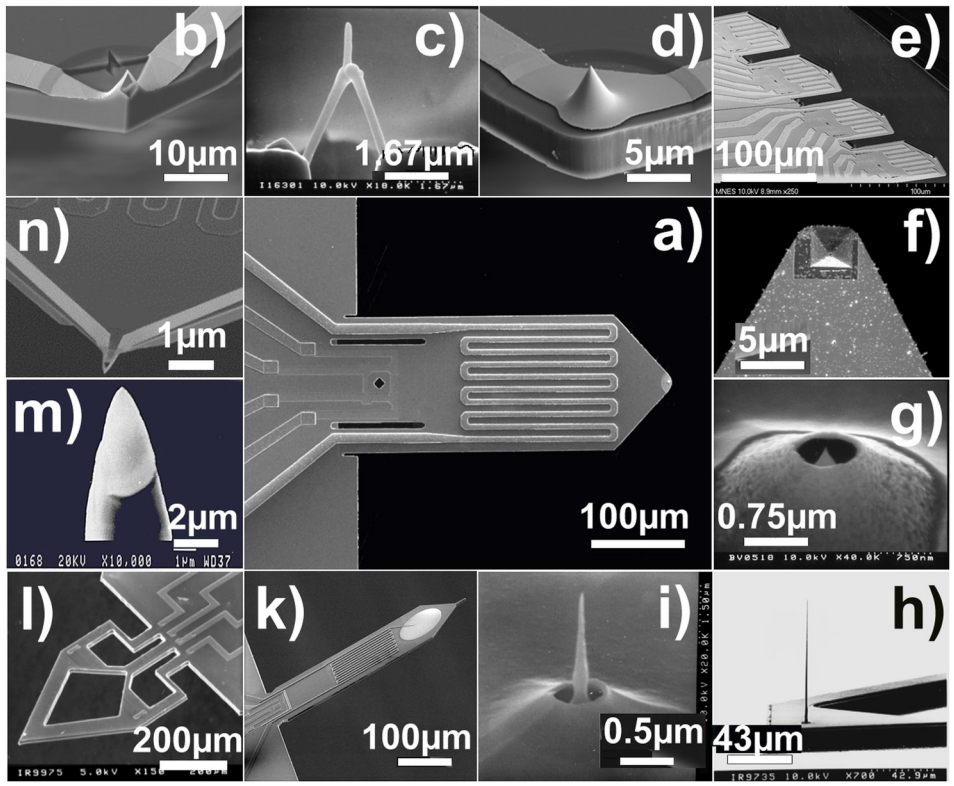

FIG. 6. (Color online) SEM image series summarizing the diversity of active cantilever modifications, targeted to specific application fields. (a) Original active cantilever type; (b)–(n) variety of tip/cantilever-functionalization. (b) Thermal-probe and AFM-probe in one [reprinted with permission from Hofer *et al.*, Microelectron. Eng. **145**, 32 (2015). Copyright 2015 by Elsevier]. (c) Thermal tip realized with EBID [reprinted with permission from Edinger *et al.*, J. Vac. Sci. Technol., B **19**, 2856 (2001). Copyright 2001 by American Institute of Physics]. (d) Conductive atomic force microscopy [reprinted with permission from Kaestner *et al.*, J. Vac. Sci. Technol., B **32**, 06F101 (2014). Copyright 2014 by American Institute of Physics]. (e) Parallel cantilever array [reprinted with permission from Sarov *et al.*, J. Vac. Sci. Technol., B **27**, 3132 (2009). Copyright 2009 by American Institute of Physics]. (f) Cantilever for single ion implantation [reprinted with permission from Ilg *et al.*, J. Vac. Sci. Technol., B **30**, 06FD04 (2012). Copyright 2012 by American Institute of Physics]. (g) Volcano-gated field emission probe [reprinted with permission from Ivanov *et al.*, J. Vac. Sci. Technol., B **19**, 2789 (2001). Copyright 2001 by American Institute of Physics]. (h) High aspect ratio cantilever tips [reprinted with permission from Rangelow *et al.*, J. Vac. Sci. Technol., B **16**, 3185 (1998). Copyright 1998 by American Institute of Physics]. (i) Coaxial SNOM tip [reprinted with permission from Kassing *et al.*, Appl. Phys. A **76**, 907 (2003). Copyright 2003 by Springer, Berlin, Heidelberg]. (k) Au-pad for biosensing applications [reprinted with permission from Kaestner *et al.*, J. Vac. Sci. Technol., B **32**, 06F101 (2014). Copyright 2014 by American Institute of Physics]. (l) Nanotribology cantilever [reprinted with permission from Gotszalk *et al.*, Ultramicroscopy **82**, 39 (2000). Copyright 2000 by Elsevier]. (m) Nanoindentation diamond tip [reprinted with permission from Rangelow *et al.*, J. Vac. Sci. Technol., B **16**, 3185 (1998). Copyright 1998 by American Institute of Physics]. (n) AFM-tip as a planar thermal loop [reprinted with permission from Hofer *et al.*, Microelectron. Eng. **145**, 32 (2015). Copyright 2015 by Elsevier].

cantilever probes are promising sensors for fast and nonoptical investigation of samples. The small tip diameter and high aspect ratio tip will ensure subnanometer topographical resolution as AFM with milli-Kelvin temperature sensitivity as thermal scanning probe. The deflection sensitivity of the integrated full Wheatstone bridge was 9.4 μV/nm, and the thermal sensitivity of thermally sensitive tip 11.2 μV/K.[34] By integration of a much smaller filament by electron beam assisted deposition (EBID) using methylcyclopentadienyl-trimethyl-platinum as a precursor gas, a thermal probe with a spatial resolution better than 80 nm and a thermal resolution of the order of 10^{-3} K has been presented [Fig. 6(c)].[35,42] The thermal-loop has a height in the range of 2–5 μm, with typical "wire" diameters between 30 and 100 nm. Because of its small size, the new probe has a high spatial resolution around 20 nm tip end radius and, due to the low thermal mass, a high thermal sensitivity and fast response time.

(3) Conductive atomic force microscopy [Fig. 6(d)]:[12] Upon the introduction of conductive tips into active probes, as shown in Fig. 6(d), a variety of measurement functions are integrated. Most significant are (a) Kelvin probe force microscopy, also known as surface potential microscopy, where the work function of surfaces is measured; (b) scanning spreading resistance microscopy method is an excellent tool for two-dimensional characterization of the free carrier distribution or dopant distribution in semiconductor devices. Moreover, we used such tips as field-emitters for the scanning probe lithography, as summarized in Sec. II F and described in Ref. 12.

(4) Parallel cantilever arrays [Fig. 6(e)]:[36] Imaging and nanofabrication with micromachined cantilevers have a limited throughput due to their serial process. Parallel operation, through arrays, can increase the working area and throughput without reducing individual cantilever performance. Two-dimensional arrays of 512,

parallel, active, independently addressable scanning proximal probes with vertical interconnections have been realized using the same CMOS/MEMS technology.[36] Figure 6(e) presents a fragment of such array. Moreover, we employed three-dimensional integration which provides significant benefits in terms of cantilever density and interconnection reduction. By using through-silicon via technology, 3D can bunch a great arrangement of functionalities into a small "footprint" of large array.

(5) Cantilever for single ion implantation: Figure 6(f)[37] presents a cantilever tip used for single ion implantation. Single dopant atoms can affect transport properties in scaled semiconductor devices. With coherent control of spin and charge degrees of freedom for single dopant atoms, quantum computing can be achieved. Single ion implantation combined with scanning probe alignment is a technique for placement of single dopant atoms with high spatial resolution and its one-by-one detection for the formation of deterministic implant structures has been demonstrated with micrometer-scale transistors and 60 keV Sb ions.

(6) Volcano-gated field emission probe [Fig. 6(g)]:[38] Here, a ring electrode surrounding the field emission scanning probe lithography nanotip is working as an electrostatic lens. As a result, the Fowler–Nordheim field emitted electron beam becomes focusable and defocusable in order to enhance the resolution or the throughput capability, respectively. In such a way, the electron beam can be generated and its size controlled.

(7) High aspect ratio cantilever tips [Fig. 6(h)]:[39] High aspect ratio cantilever tips were developed as a novel combination of silicon micromachining and deposition of silicon whiskers on (111) oriented silicon substrates. These tips show promise for stable field emission electron emitters for SPL and sensors for AFM. These tips used as field emission electron emitter demonstrate great potential for high-density and high-resolution electron beam applications owing to a small (within 3°) divergence half angle of emitted electrons.

(8) Coaxial scanning nearfield optical microscope (SNOM) tip [Fig. 6(i)]: SNOM is a noticeable member of the scanning probe microscopy techniques.[43,44] The motivator behind this technology is based on the possibility to circumvent the optical diffraction limit of conventional optical microscopy. In this approach, the light enters the hollow tip and an evanescent wave emerges from the aperture. In contrary to conventional microscopy, the diameter of the aperture determines the resolution rather than the wavelength. However, a problem of the aperture-based SNOM is the extreme intensity of the evanescent wave. For that reason, a coaxial sensor has been fabricated.[40]

(9) Au-pad for biosensing applications [Fig. 6(k)]: An Au-Pad integrated onto the active cantilever can be used for bio-sensing applications enabling specific binding to target molecules as bio-recognition elements with high affinity.

(10) Nanotribology cantilever [Fig. 6(l)]:[41] Tribology cantilever delivering topology and tribological information consists of a micromachined silicon cantilever beam with an integrated microtip and piezoresistive sensors for detecting the lateral and vertical forces acting on the tip. We have also demonstrated the possibility of three-dimensional complex surface characterization by means of the modified AFM/lateral force microscopy active cantilever sensor. Moreover, the use of this kind of "intelligent" probes can contribute in the phenomenological understanding of adhesion, tribology, and interfacial/fracture mechanics.

(11) Nanoindentation diamond tip [Fig. 6(m)]: Active cantilevers were equipped with single crystal diamond tip grown onto vapor–liquid–solid silicon whiskers, which is useful for a nanoindentation of materials. Moreover, the diamond coating stabilizes and increases a field-emission current up to 100 μA from a single tip.[39]

In addition to the above mentioned applications, by controlling the interaction strength between the probe tip and the sample, it is also possible to fabricate well-defined nanoscale structures. As such, self-actuated and self-sensed probes can also be used as important tools in the fabrication of the next generation nanoelectronic devices, discussed next. Here, in the last decade, a set of scanning probe tools for alternative lithographic techniques have been developed.[45]

E. Field emission scanning probe lithography

The ability of rapid nanoscale manufacturing in single digit nanoscale, in a reproducible manner, has been identified as one of the most essential steps to enable future nanoelectronic,[46] nanoelectromechanical systems, photonic, and bio-nanotechnology-based devices. In this context, the establishment of two fundamental technologies for the sub-10 nm scale is required: lithography and pattern transfer. In order to address this challenge, we recently developed a novel lithographic technology based on scanning probe technology, so called FE-SPL. Here, a beam of low energy electrons, field-emitted from the apex of an active scanning proximal probe tip, is capable to induce highly confined positive and negative tone as well as self-development reactions within ultrathin molecular resist layers. This is combined with pattern transfer techniques, especially cryogenic etching, enabling pattern transfer toward single digit nanofeatures.

Within the FE-SPL concept, schematically drawn in Fig. 7, a high electric field is applied in order to induce a Fowler–Nordheim emission[47] from a scanning proximal probe tip. Due to the low electron energies, typically $\leq$50 eV, which are close to the binding energies of the resist molecules, the lithographic process is efficient and proximity effects are circumvented.[48,49] Lithographic processes, which are spatially confined to the sub-10 nm scale are yielded by the highly localized electric field and the use of tip-sample distances well below 100 nm. Based on the thermomechanically actuated, piezoresistive, so called active cantilever technology[14,50] a scanning probe lithography

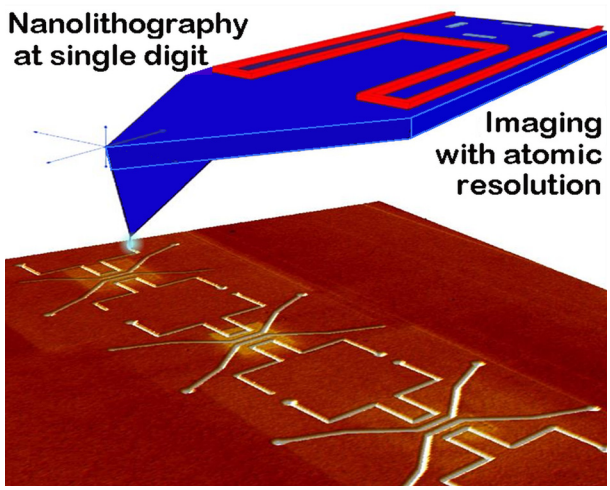

FIG. 7. (Color online) Concept of field emission scanning probe lithography incorporating AFM imaging and FE-SPL patterning.

platform[18,50] able to image, inspect, align and pattern features at the single-digit nanoregime was developed. A corresponding example, patterned in positive tone development-less mode, is summarized in Fig. 8. Here, a variable grid structure with a pitch modulation from 15 to 25 nm hp (half-pitch) is patterned. AFM topographic imaging is carried out directly after patterning, without application of intermediate steps, by using the same cantilever.

In frame of our research on FE-SPL, we demonstrated: (1) a closed-loop lithography for generation of lithographic features in positive, negative as well as in dual tone;[12,18,50] (2) a novel self-development mode, wherein the resist material is directly removed, which avoids development-related problems;[17,18,48,49] (3) sub-10 nm lithographic resolution capabilities; [17,18] (4) step-and-repeat, multistep, and multilayer lithography by incorporation of probe-based high accuracy alignment;[18,19] (5) applicability of novel molecular glass resists and coevaporated resist material systems;[51,52] (6) patterning of 2D-materials, e.g., MoS^2 nanoribbons with 15 nm lateral confinement; (7) pattern transfer capability of FE-SPL defined features by plasma etching at cryogenic temperatures.[29,53]

As a main result, the developed technology chain has demonstrated its capability by successful fabrication of room-temperature single electron transistor (SET) devices showing effective quantum dot sizes of less than 2 nm. Beyond, the successful replication of FE-SPL patterned master templates of SET devices by using nanoimprint lithography (NIL) demonstrated the capability to proceed toward high throughputs.

Additionally, in order to enhance the throughput capability of FE-SPL, further improvements were achieved: (8) progress with respect to AFM imaging speed using active cantilever;[30,54,55] (9) upscaling of the lithographic process by using four independently addressable and controllable active cantilever;[56] (10) investigation of volcano-gated nanoprobes for FE-SPL to focus and defocus the electron beam in order to enhance the resolution or the throughput capability, respectively;[57] (11) complementary mix and match lithography, wherein FE-SPL is applied for highest resolution critical dimension patterning;[17] and (12) combination of FE-SPL

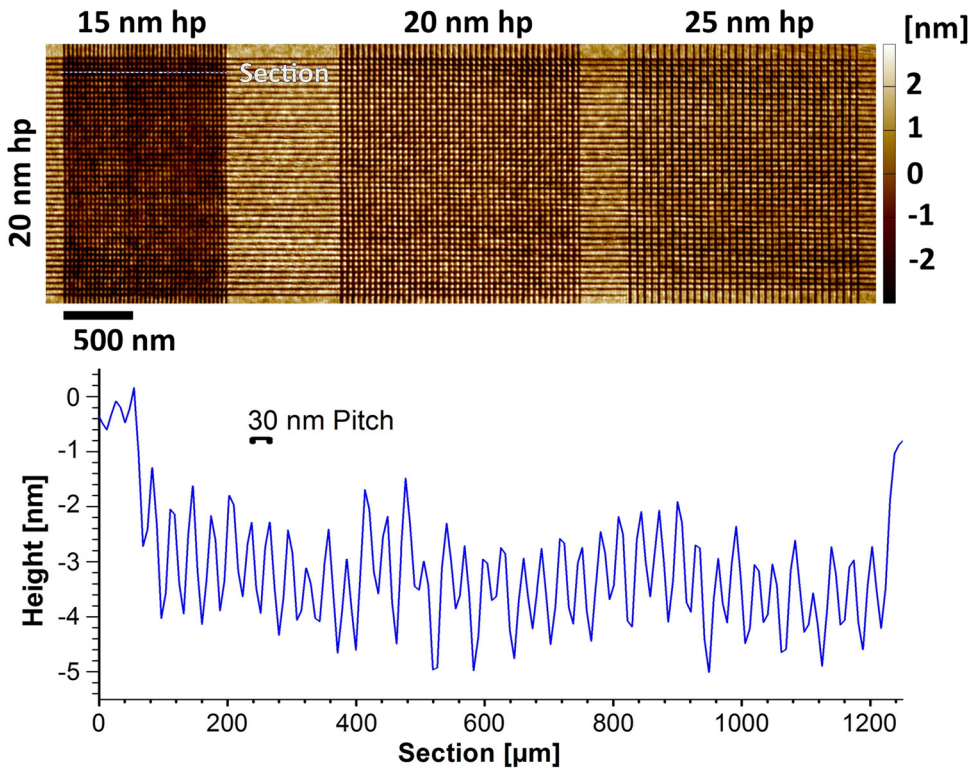

FIG. 8. (Color online) Variable grid structure patterned by FE-SPL in ~5 nm thick molecular resist. The pitch of the vertical lines was modulated from 15up to 25 nm hp. The horizontal parallel lines were patterned with a constant half-pitch of 20 nm.

with NIL. In this concept, the master template was made by a combination of standard optical lithography and FE-SPL in a so called mix and match process.

III. PARALLELIZATION AND SCANNER OPTIMIZATION FOR HIGH-SPEED AFM USING ACTIVE PROBES

As discussed in Sec. II, high-speed nanoscale manipulation (e.g., fabrication) and visualization (microscopy) performance are demanded in microelectronics, material sciences, as well as in biology. However, these applications need to satisfy very different requirements. In biology, in case of video-rate visualization of protein dynamics, the topographic height variations are often bounded to a few nanometers. Similarly, to capture several proteins in the same field of view, a scan range in the order of tens of nanometers is absolutely sufficient. Similar values, although slightly higher, are required in material sciences, e.g., study of the dissolution of crystal monolayers in various solvents. However, these specifications are far from meeting the requirements of micro/nanoelectronics, where lateral ranges in the order of hundreds of microns ($>500\,\mu$m) and an out of plane range around 20–30 μm may be needed. In a similar fashion, when it comes to imaging speed, the microelectronics industry has the most stringent requirements, since the evaluation of thousands of features placed across a full silicon wafer is targeted. To clarify the requirements and their associated challenges across various industries, in the following, we discuss in detail the meanings of high-speed scanning probe microscopy.

One of the biggest targets of high speed AFM imaging is the capturing of images at high frame rates, ideally at video rates. Due to the difference in physical imaging in terms of resolution, scan range, sample topography, and associated variation of spatial frequency by using only the frame rate as the sole parameter to determine imaging speed performance is not accurate. Since "high-speed" is not clearly defined, we attempt to give a unified framework for performance comparison between "high-speed" AFM imaging by identifying the relationship between important imaging parameters. In the following, we propose a method for comparison between different AFM systems.

A. Imaging parameters and their relation to scanner bandwidth

During the capturing of a scanning probe microscopy video, there are numerous criteria that can be utilized for characterization of its quality. In the case of high speed atomic force microscopy, the frame rate F_r, imaging range L, resolution R, and minimum traceable sample spatial wavelength λ are key parameters. From a scanner design point of view, the maximum BW for each axis, which can be achieved for the specified operation range, is important.

In order to get a closed form governing equation, we assume that the sample surface topography is composed of a sinusoidal spatial variation. The governing equations, assuming sinusoidal driving frequency, are given by

$$F_r \leq 2 \cdot \mathrm{BW}_y, \tag{4}$$

$$F_r \cdot R_y \leq 2 \cdot \mathrm{BW}_x, \tag{5}$$

$$\frac{F_r \cdot R_y \cdot L_x}{\lambda_{min}} \leq C_z \cdot \mathrm{BW}_z, \tag{6}$$

where F_r is the frame rate of the video in hertz, R_y is the resolution [pixel] along the Y direction (= number of lines to be scanned), L_x is the imaging range in X axis direction (nm), λ is the smallest spatial wavelength (nm) of the sample topography, which can be captured, BW_x and BW_y are the scanning bandwidth in X and Y direction, respectively, BW_z is the Z axis controller bandwidth, and C_z is a dimensionless proportionality constant that depends on the imaging condition. For example, in tapping mode, C_z is typically chosen as $C_z = 2\theta_m/\pi$, with θ_m the maximum phase lag allowed for the sample.[58]

The relation between scanner range, resolution, and spatial frequency of a surface topography is shown exemplarily in Fig. 9. The following parameters were chosen: $\mathrm{BW}_x = 10\,\mathrm{kHz}$, $\mathrm{BW}_y = 300\,\mathrm{Hz}$, $\mathrm{BW}_{zc} = 100\,\mathrm{kHz}$, $K_x = 1$, $K_y = 1$, and $C_z = 1$. We assume that the scan range and resolution are same in X and Y directions, which gives $L_x = L_y$ and $R_x = R_y$. The vertical axis gives the spatial frequency defined as $1/\lambda$.

B. Comparison between AFM systems

Due to different imaging ranges, resolution, and sample property requirements, AFM sample scanners are designed to target different imaging conditions. Scanners with a smaller range, i.e., a few microns, have higher bandwidth (up to more than 100 kHz) while larger scanners featuring ranges over 100 μm usually have a bandwidth of several hundred hertz.

Despite the difference in range and bandwidth, the product between the bandwidth and range of operation characterizes the maximum scanning speed. The maximum in-plane tracking speed $V_{x,\max}$ and vertical tracking speed $V_{z,\max}$ and their relation can be obtained as follows:

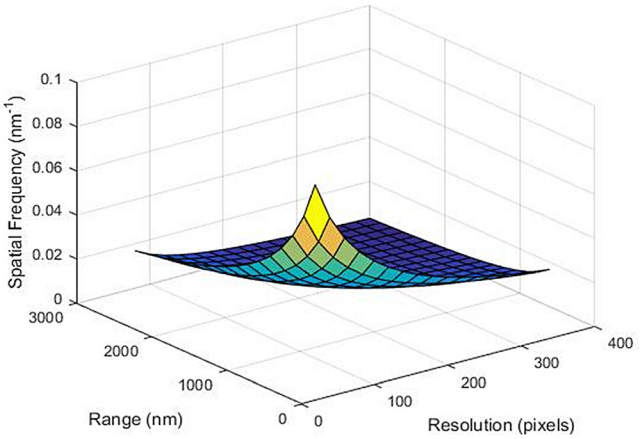

FIG. 9. (Color online) Relation between scanner range, resolution, and spatial frequency for 25 frames per second (fps).

$$V_{x,\max} = 2\mathrm{BW}_x \cdot D_x, \tag{7}$$

$$V_{z,\max} = 2\mathrm{BW}_z \cdot D_z, \tag{8}$$

$$V_{z,\max} \geq \frac{4S_z}{\lambda} \cdot V_{x,\max}, \tag{9}$$

where BW_x and BW_z are the X axis and Z axis tracking bandwidth, D_x and D_z are the operation range corresponding to the bandwidth utilized in the equation, and S_z is the amplitude of the sample topography variation. Thus, we see that both $V_{x,\max}$ and $V_{z,\max}$ can limit the maximum imaging speed. Whether $V_{x,\max}$ or $V_{z,\max}$ is the actual limit depends on the sample topography variation. Even if we can obtain a very large $V_{x,\max}$, the tracking speed is still limited by the value of $V_{z,\max}$. On the other hand, for a flat surface, where $S_z = 0$, $V_{x,\max}$ sets the limitation. By utilizing the value of both $V_{x,\max}$ and $V_{z,\max}$, we can compare the performance of an AFM imaging system for a given sample with a certain topographic variation.

In addition, based on all imaging parameters as discussed earlier, the in-plane scanning velocity of an AFM video can be calculated. The out of plane tracking speed can be estimated by summing up the absolute values of differences between two consecutive topographic height measurements, divided by the total time required for taking these pixels. On the basis of this information, one can characterize the AFM video imaging speed across various schemes of applications with different imaging ranges, resolution, and sample topography variation requirements.

C. AFM with arrays of active cantilevers

In addition to probe fabrication, we have developed novel methods as fast cantilever-approach technology and novel adaptive scanning speed procedure[30,54] to obtain high-speed AFM. Furthermore, in order to significantly enhance the imaging throughput, we work on the upscaling by using cantilever arrays. Recently, we have developed a so called "Quattro" cantilever array system, wherein four active cantilevers are operating simultaneously.[57] The "Quattro" cantilever array is shown in Fig. 10. An example of an AFM image, acquired with the "Quattro" cantilever array system, is shown in Fig. 11. The "Quattro" cantilever array technology is a very powerful imaging device with an effective imaging speed of about 5 mm/s over a relatively large range. These characteristics make our technology suitable for a wide range of novel applications, e.g., for semiconductor quality control or high-throughput nanofabrication.

The distance between the tips of the neighboring active probes in a "Quattro" cantilever array is 125 μm.[53] To realize the full promise of this technology for high-throughput applications, the lateral scan range should be larger than the probe spacing. Across such a large lateral motion, the out-of-plane positioning range of self-actuating probes is not large enough in order to handle large topological variations, e.g., caused by a sample tilt. In order to circumvent this issue, we combine microactuated cantilevers with high-speed "macro" piezoactuators. Therefore, a multiactuated nanopositioner with more than 125 μm lateral range and several microns of out-plane-range[20,59] was developed, described in Sec. III D. By combining the actuation capability of our micro- and nanopositioning systems, we are able to simultaneously meet the range and speed requirements of more challenging applications, e.g., in surface engineering or in high-throughput nanolithography for single-digit nanodevices.

D. High-speed large-range scanner design

The scanner is a key unit needed to be optimized for high-speed imaging. The essential steps toward high-speed scanners are as follows:

(1) to minimize parasitic vibrations;
(2) to eliminate the impulse forces effects, which are generated in consequence of the piezo-stack displacements;
(3) to move the resonance frequencies toward higher frequencies; and
(4) to damp and reduce the quality factor.

Usually, a good solution is to support a piezo-stack at both ends with stiff flexures. Aspects to be addressed in the

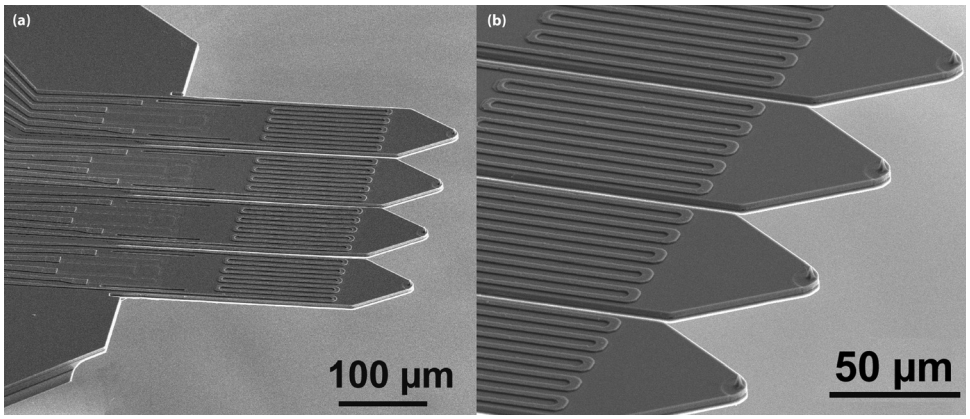

FIG. 10. Active cantilever "Quattro" array (a) and fragment of very end of the cantilevers shows the quality and positioning accuracy of AFM-tips (b). The height of the silicon-tips is 6 μm.

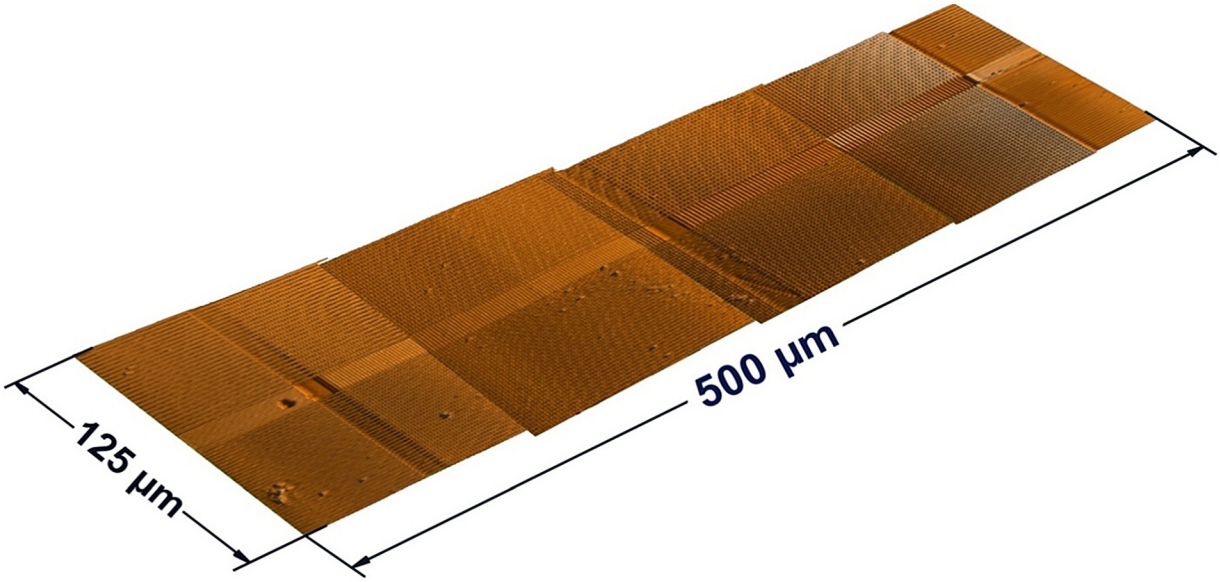

FIG. 11. (Color online) Parallel imaging with a Quattro cantilever array: Four AFM topographic images are stitched together, which were obtained by simultaneous operation of four active cantilevers applied in the Quattro-array AFM setup.

design of a high-speed and large-scale scanner are as follows:

(1) The scanner must be able to compensate a slowly changing topography, which is caused by sample tilt.
(2) A multiactuated scanner axis should be utilized in order to allow imaging of a small area at higher speeds, in addition to the large area imaging.
"Quattro" cantilever arrays should be integrated into the scanner, which necessitates the movement of the probes instead of the sample. This opens up
(3) the possibility for imaging of large samples, which conventionally cannot be positioned at high speeds.

In the following paragraphs, the scanner design, according to the above described aspects, is described. In order to cover the imaging of large areas at slower scanning speeds, a commercially available P-517.3CL positioning system in the first experiment is utilized. This scanner type offers in X and Y directions a travel range of 130 μm and a bandwidth of 450 Hz. In Z axis direction, a travel range of 25 μm with 1100 Hz bandwidth is given. Thereby, the integration of a high-speed, short range positioning option for the X axis is useful for small area high frame rate video imaging. The high-speed X positioning system is designed by using two P-885.11 piezo actuators delivering a scan range of 6 μm. The assembled system is shown in Fig. 12. The central stage can be utilized to host an additional Z axis high speed positioner, which is able to achieve scan ranges of up to 1 μm at 100 kHz bandwidth. Alternatively, an enlarged Z axis scan range of 4 μm can be achieved, which is linked to a decreased bandwidth of 20 kHz.

The bandwidth for the X axis is 10 kHz with associated Bode plot from system identification using binary stochastic signal input shown in Fig. 13.

The last aspect addresses the "Quattro" cantilever array positioning stage. This allows samples of larger

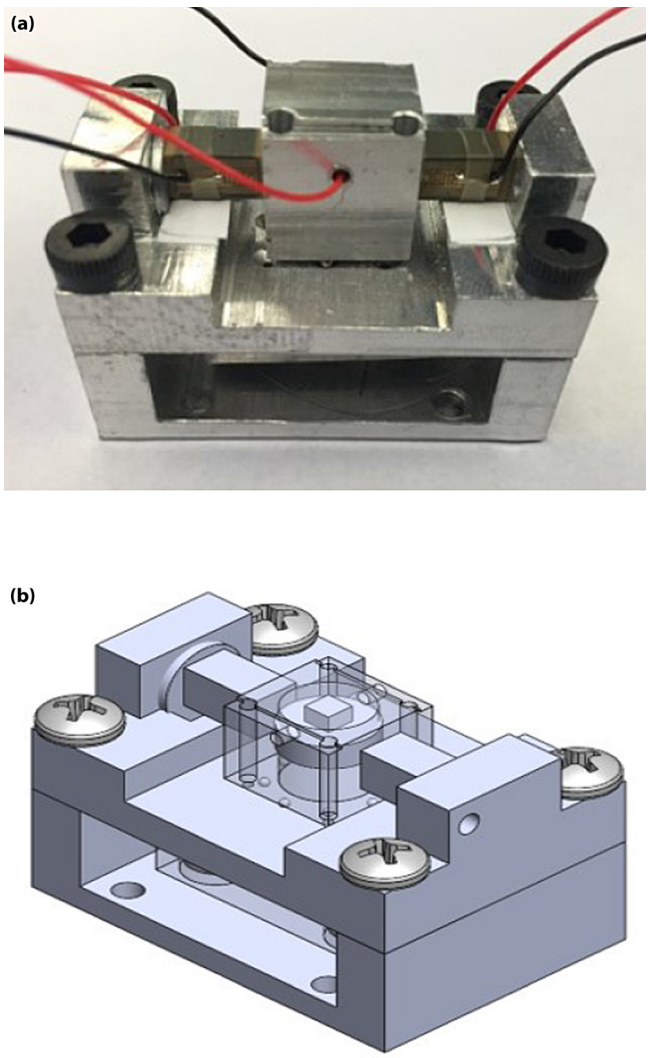

FIG. 12. (Color online) Z_1 and X_1 axis positioner structure assembly.

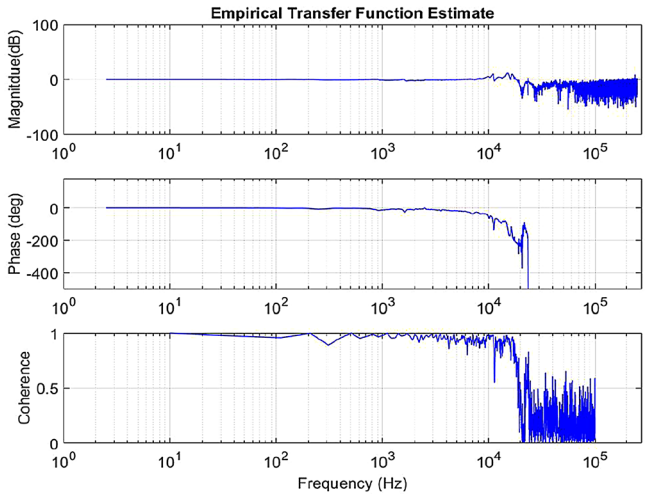

FIG. 13. (Color online) *X* axis bode plot for dual actuated *X* axis scanner design.

geometric sizes to be imaged at high speed as the mass carried by the scanner is independent of the sample. The accompanied solution is to incorporate an adapter to the sample stage to mount the "Quattro" cantilever array as shown in Fig. 14.

E. Applied scanner control strategy

For slow axis operation, a model based feed-forward compensation is utilized in order to tackle the problem of piezo hysteresis. If a higher positioning accuracy is needed, a displacement signal measurement from capacitive sensors can be utilized for feedback. At high speed operation, it is hard to apply the conventional hysteresis model inversion control for piezo hysteresis compensation due to its computational complexity. To achieve high bandwidth scanning, sinusoidal scanning patterns can be utilized instead of triangular scanning pattern to avoid high frequency dynamics caused by the sharp turning.[59] In addition, sinusoidal scanning pattern opens the possibility for using repetitive control algorithm. By designing proper controller following the internal model principal, a large gain at the driving sinusoidal frequency can be added to the system to eliminate tracking error.[60,61] A data-based control strategy is used for compensation of the coupled dynamics, whereby at the same time it divides the positioning responsibility between multiple actuators. Since during the scanner design step we ensured minimal dynamic coupling, the designed compensators are easy to implement. All compensation components are designed auxiliary to a PID unit. In this form, although the combined controller can be very complex (high-order), from the user's perspective the same gains are tuned as in conventional scanning probe microscopes.[20] Since for every single actuator a separate compensator is needed, the design can be implemented in a sequential manner, starting with the slowest actuator moving toward higher frequencies.

IV. SUMMARY AND CONCLUSIONS

Small active probes have emerged as one of the essential cost-effective methodologies in the fabrication of nanoscale

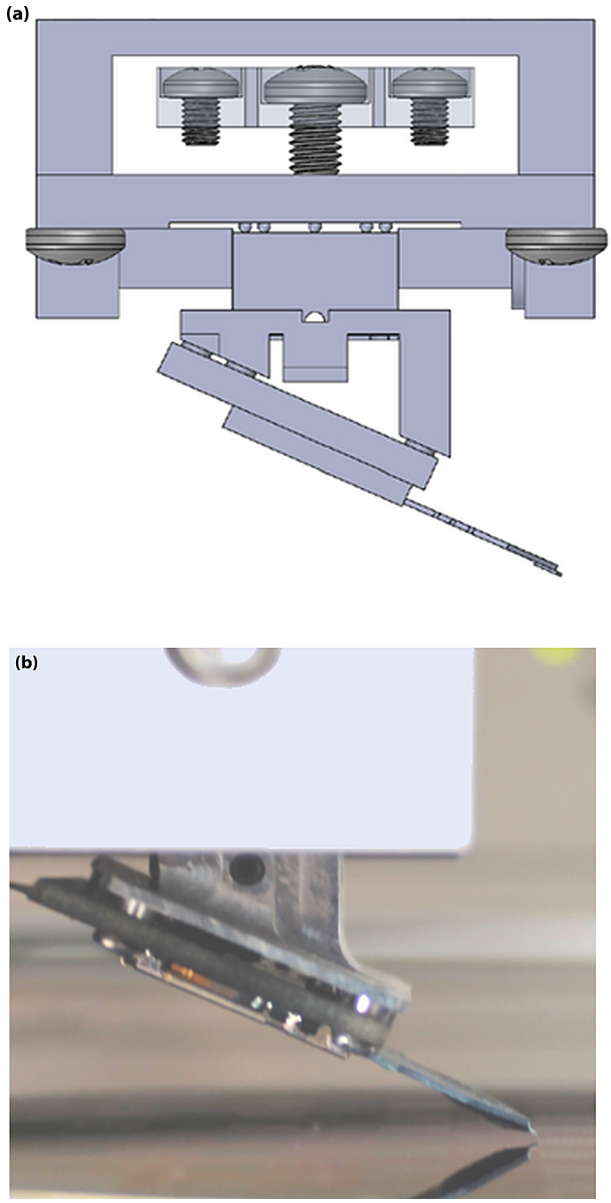

FIG. 14. (Color online) Probe positioning and cantilever auto-approach system integrating a four cantilever array chip.

structures due to their advantages as lithography resolution capabilities and high-speed operation. Piezoresistive probes are comparable to passive probes using optical read-out when considering AFM applications. MEMS-technology based down-scaling of the cantilever dimensions and improved design made it possible to generate high strain in the place where the cantilever piezoresistors are localized and reduce the cross talk between sensor and actuator to a negligible level. In such manner, active probes are applicable for high-speed imaging of features with high aspect ratio at a very low rapid tip wear. Moreover, the technological advances in piezoresistive strain sensing make this type of cantilever suitable for force sensing and ultimately sensitive for deflection sensing. Thus, active probes are able to routinely obtain atomic step resolution at a low thermal noise floor.

The self-actuated piezoresistive cantilevers allow for easier system integration and significant reduction in the systems weight. Microscopes incorporating them offer a better controllability and significantly better imaging throughput. Furthermore, in contrast to conventional optical read-out systems, these systems offer the potential for full lithographic and metrological automation. For FE-SPL, the implemented AFM-mode enables an *in situ* inspection capability, a quantitative mapping at unprecedented resolution, as well as an integrated overlay alignment system.

In this review, we further highlighted the importance of piezoresistive cantilevers with integrated actuator elements. The manifested merits of their use include the simplicity of microelectronic architecture, the enhanced controllability of analytical image processing, the ability of full automation, and the detection of very minute sample interactions (mechanical, electrical, thermal, and chemical), with significant reduction of the setup processes. These properties make this approach more efficient as opposed to optical read-out techniques. The potential of active cantilevers provides significant economic benefits and it is confirmed by the interest throughout industry and science institutions.

Finally, we discussed the potentials of combined application of micro- and macroactuators and the merits of multiactuation methodologies. In our proposed approach, we combined several short-range/high-speed and large-range/slow nanopositioners to achieve range and speed requirements in more recent applications. Self-actuated cantilever probes are included among the applied nanopositioners adding an unforeseen range and speed performance to our system. The control design of such a multicomponent system can be very complex, especially in the presence of dynamic coupling. We discussed the possibility of design techniques to minimize such interactions and further design of compensation controllers as auxiliary components to PID unit. This further simplifies the application of the instrument.

ACKNOWLEDGMENTS

This project has received funding from the European Union's Seventh Framework Program for research, technological development and demonstration under Grant Agreement No. 318804 [Single Nanometer Manufacturing (SNM) for beyond CMOS devices] and Thüringer Aufbaubank Project No. 6343. This work was also supported by the center for clean water and clean energy at the Massachusetts Institute of Technology. The authors would like to express their gratitude to Teodor Gotszalk from the Wroclaw University of Technology and to Piort Grabiec from the Institute of Electron Technology (ITE) in Warsaw for the fruitful and excellent cooperation.

[1]H. J. Butt, P. Siedle, K. Seifert, K. Fendler, T. Seeger, E. Bamberg, A. L. Weisenhorn, K. Goldie, and A. Engel, J. Microsc. **169**, 75 (1993).
[2]Y. L. Lyubchenko, L. S. Shlyakhtenko, and T. Ando, Methods **54**, 274 (2011).
[3]T. Ando, N. Kodera, E. Takai, D. Maruyama, K. Saito, and A. Toda, Proc. Natl. Acad. Sci. U. S. A. **98**, 12468 (2001).
[4]H. Hu, H. Joon Kim, and S. Somnath, Micromachines **8**, 90 (2017).
[5]Y. K. Yong, S. P. Wadikhaye, and A. J. Fleming, Rev. Sci. Instrum. **87**, 085104 (2016).
[6]M. Maroufi, A. Bazaei, and S. O. R. Moheimani, IEEE Trans. Control Syst. Technol. **23**, 504 (2015).
[7]D. A. Walters, J. P. Cleveland, N. H. Thomson, and P. K. Hansma, Rev. Sci. Instrum. **67**, 3583 (1996).
[8]T. E. Schäffer, J. P. Cleveland, F. Ohnesorge, D. A. Walters, and P. K. Hansma, J. Appl. Phys. **80**, 3622 (1996).
[9]M. B. Viani *et al.*, Rev. Sci. Instrum. **70**, 4300 (1999).
[10]Y.-P. Song, S. Wu, L.-Y. Xu, J.-M. Zhang, D. J. Dorantes-Gonzalez, X. Fu, and X.-D. Hu, Meas. Sci. Technol. **26**, 065001 (2015).
[11]G. Binnig, C. Quate, and C. Gerber, Phys. Rev. Lett. **56**, 930 (1986).
[12]M. Kaestner *et al.*, J. Vac. Sci. Technol., B **32**, 06F101 (2014).
[13]I. W. Rangelow, J. Vac. Sci. Technol., B **21**, 1550 (2003).
[14]T. Angelov, D. Roeser, T. Ivanov, S. Gutschmidt, T. Sattel, and I. W. Rangelow, Microelectron. Eng. **154**, 1 (2016).
[15]T. Michels and I. W. Rangelow, Microelectron. Eng. **126**, 191 (2014).
[16]A. A. Tseng, *Tip-Based Nanofabrication* (Springer Verlag, New York, 2011).
[17]M. Kaestner, M. Hofer, and I. W. Rangelow, J. Micro/Nanolithogr. MEMS MOEMS **12**, 031111 (2013).
[18]M. Kaestner *et al.*, J. Micro/Nanolithogr. MEMS MOEMS **14**, 031202 (2015).
[19]V. Ishchuk *et al.*, Appl. Phys. A **123**, 89 (2017).
[20]I. Soltani Bozchalooi, A. Careaga Houck, J. M. AlGhamdi, and K. Youcef-Toumi, Ultramicroscopy **160**, 213 (2016).
[21]I. Soltani Bozchalooi and K. Youcef-Toumi, *Proceedings of the ACC Conference* (2014), p. 1643.
[22]I. Soltani Bozchalooi, A. Houck, and K. Youcef-Toumi, *Proceedings of the ACC Conference* (2015), p. 3478.
[23]F. Xia, I. Soltani Bozchalooi, and K. Youcef-Toumi, *Proceedings of the ACC Conference* (2017), p. 4141.
[24]M. Tortonese, H. Yamada, R. C. Barrett, and C. Quate, *Proceedings of the 2nd International Conference on Solid-State Sensors and Actuators (Transducers'91)* (1991), p. 448.
[25]I. W. Rangelow, S. Skocki, and P. Dumania, Microelectron. Eng. **23**, 365 (1994).
[26]P. L. P. Hoa, G. Suchaneck, and G. Gerlach, Sens. Actuators, A **120**, 567 (2005).
[27]R. Linnemann, T. Gotszalk, L. Hadjiiski, and I. W. Rangelow, Thin Solid Films **264**, 159 (1995).
[28]R. Pedrak, T. Ivanov, T. Gotszalk, P. Hudek, O. Fortagne, and I. W. Rangelow, J. Vac. Sci. Technol., B **21**, 3102 (2003).
[29]I. W. Rangelow *et al.*, J. Vac. Sci. Technol., B **34**, 06K202 (2016).
[30]A. Ahmad, T. Ivanov, T. Angelov, and I. W. Rangelow, J. Micro/Nanolithogr. MEMS MOEMS **14**, 031209 (2015).
[31]I. Rangelow, T. Ivanov, P. Hudek, and O. Fortagne, U.S. patent 2005225011 (13 October 2005).
[32]B. Ilic, S. Krylov, and H. G. Craighead, J. Appl. Phys. **107**, 034311 (2010).
[33]T. Michels, E. Guliyev, M. Klukowski, and I. W. Rangelow, Microelectron. Eng. **97**, 265 (2012).
[34]M. Hofer, T. Ivanov, M. Rudek, D. Kopiec, E. Guliyev, T. P. Gotszalk, and I. W. Rangelow, Microelectron. Eng. **145**, 32 (2015).
[35]K. Edinger, I. W. Rangelow, and T. Gotszalk, J. Vac. Sci. Technol., B **19**, 2856 (2001).
[36]Y. Sarov *et al.*, J. Vac. Sci. Technol., B **27**, 3132 (2009).
[37]M. Ilg *et al.*, J. Vac. Sci. Technol., B **30**, 06FD04 (2012).
[38]T. Ivanov, I. W. Rangelow, and S. Biehl, J. Vac. Sci. Technol., B **19**, 2789 (2001).
[39]I. W. Rangelow *et al.*, J. Vac. Sci. Technol., B **16**, 3185 (1998).
[40]R. Kassing, I. W. Rangelow, E. Oesterschulze, and M. Stuke, Appl. Phys. A **76**, 907 (2003).
[41]T. Gotszalk, P. Grabiec, and I. W. Rangelow, Ultramicroscopy **82**, 39 (2000).
[42]M. Joodaki, P. Janus, T. Gotszalk, G. Kompa, K. Edinger, and I. W. Rangelow, Jpn. J. Appl. Phys., Part 1 **44**, 6823 (2005).
[43]D. W. Pohl, W. Denk, and M. Lanz, Appl. Phys. Lett. **44**, 651 (1984).
[44]P. Grabiec, J. Radojewski, M. Zaborowski, K. Domanski, T. Schenkel, and I. W. Rangelow, J. Vac. Sci. Technol., B **22**, 16 (2004).
[45]A. A. Tseng, A. Notargiacomo, and T. P. Chen, J. Vac. Sci. Technol., B **23**, 877 (2005).
[46]Z. Durrani, M. Jones, M. Kaestner, M. Hofer, E. Guliyev, A. Ahmad, T. Ivanov, J. P. Zoellner, and I. W. Rangelow, Proc. SPIE **8680**, 868017 (2013).

[47]S. Lenk, M. Kaestner, C. Lenk, T. Angelov, Y. Krivoshapkina, and I. W. Rangelow, J. Nanomater. Mol. Nanotechnol. **5**, 6 (2016).
[48]M. Kaestner and I. W. Rangelow, J. Vac. Sci. Technol., B **29**, 06FD02 (2011).
[49]M. Kaestner and I. W. Rangelow, Microelectron. Eng. **97**, 96 (2012).
[50]M. Kaestner *et al*., Proc. SPIE **9049**, 90490C (2014).
[51]C. Neuber *et al*., Proc. SPIE **9049**, 90491V (2014).
[52]C. Neuber *et al*., Proc. SPIE **9425**, 94250E (2015).
[53]V. Ishchuk, D. L. Olynick, Z. W. Liu, and I. W. Rangelow, J. Appl. Phys. **118**, 053302 (2015).
[54]A. Ahmad, A. Schuh, and I. W. Rangelow, Rev. Sci. Instrum. **85**, 103706 (2014).
[55]A. Schuh, M. Hofer, T. Ivanov, and I. W. Rangelow, J. Microelectromech. Syst. **24**, 1622 (2015).
[56]A. Ahmad *et al*., J. Vac. Sci. Technol., B **34**, 06KM03 (2016).
[57]S. Lenk, M. Kaestner, C. Lenk, and I. W. Rangelow, Microelectron. Eng. **177**, 19 (2017).
[58]T. Ando, FEBS Lett. **587**, 997 (2013).
[59]I. Soltani Bozchalooi and K. Youcef-Toumi, Ultramicroscopy **146**, 117 (2014).
[60]M. Bodson, A. Sacks, and P. Khosla, IEEE Trans. Automatic Control **39**, 1939 (1994).
[61]T. Sakanushi, K. Yamada, I. Murakami, Y. Ando, T. Hagiwara, S. Matsuura, and J. Hu, Int. J. Innovative Comput. **8**, 4883 (2012).